

## Thermal consequences of impacts in the early solar system

Fred J. CIESLA<sup>1\*</sup>, Thomas M. DAVISON<sup>2</sup>, Gareth S. COLLINS<sup>2</sup>, and David P. O'BRIEN<sup>3</sup>

<sup>1</sup>Department of the Geophysical Sciences, University of Chicago, 5734 South Ellis Avenue, Chicago, Illinois 60637, USA

<sup>2</sup>Impact and Astromaterials Research Centre, Department of Earth Science and Engineering,  
Imperial College London, London, UK

<sup>3</sup>Planetary Science Institute, 1700 E. Fort Lowell, Suite 106, Tucson, Arizona 85719, USA

\*Corresponding author: E-mail: fciesla@uchicago.edu

(Received 23 January 2013; revision accepted 21 October 2013)

---

**Abstract**—Collisions between planetesimals were common during the first approximately 100 Myr of solar system formation. Such collisions have been suggested to be responsible for thermal processing seen in some meteorites, although previous work has demonstrated that such events could not be responsible for the global thermal evolution of a meteorite parent body. At this early epoch in solar system history, however, meteorite parent bodies would have been heated or retained heat from the decay of short-lived radionuclides, most notably <sup>26</sup>Al. The postimpact structure of an impacted body is shown here to be a strong function of the internal temperature structure of the target body. We calculate the temperature–time history of all mass in these impacted bodies, accounting for their heating in an onion-shell-structured body prior to the collision event and then allowing for the postimpact thermal evolution as heat from both radioactivities and the impact is diffused through the resulting planetesimal and radiated to space. The thermal histories of materials in these bodies are compared with what they would be in an unimpacted, onion-shell body. We find that while collisions in the early solar system led to the heating of a target body around the point of impact, a greater amount of mass had its cooling rates accelerated as a result of the flow of heated materials to the surface during the cratering event.

---

### INTRODUCTION

Meteorites are largely derived from asteroids, the leftover planetesimals that formed in the terrestrial planet region of our protoplanetary disk, the solar nebula, over 4.5 billion years ago. As such, these bodies provide an important record of the conditions that were present and processes that operated during the early epoch of planet formation. This record includes evidence of heating in the form of differentiation, melt pools, and metamorphism, which have largely been attributed to the decay of short-lived radionuclides (SLRs), with <sup>26</sup>Al being the most important (see Ghosh et al. [2006] for a recent review). Indeed, models for the warming of asteroidal-sized bodies by <sup>26</sup>Al predict that melting and differentiation (e.g., Ghosh and McSween 1998; Hevey and Sanders 2006; Qin et al. 2008; Elkins-Tanton et al. 2011) or the thermal metamorphism seen in the unmelted chondritic meteorites (Grimm and

McSween 1993; Trierloff et al. 2003; Kleine et al. 2008; Harrison and Grimm 2010) would be widespread and begin in the first approximately 5 Myr of solar system history, with radiogenic heat being retained for 0.1–1 Gyr.

While the decay of <sup>26</sup>Al is believed to have been the primary heating mechanism in early planetesimals, impacts have also been discussed as a potential heat source. Impacts have been invoked to explain thermal events that occurred late (>10 Myr) into solar system history (Schulz et al. 2009, 2010, 2012), the juxtaposition of melted and heavily metamorphosed chondritic rocks (Rubin 1995), and the correlations between petrologic type and shock stage in ordinary chondrites (Rubin 2003, 2004). Indeed, the asteroid belt has undergone significant collisional evolution over its lifetime and, particularly, in its nascent stage (e.g., O'Brien and Sykes 2011), making impacts an appealing source of heat in meteorite parent bodies.

However, previous studies demonstrated that impacts would have been unable to drive the global-scale thermal evolution inferred for meteorite parent bodies. Keil et al. (1997), based in part on the numerical simulations of Love and Ahrens (1996), concluded that global-scale temperature changes from impacts would be on order of approximately 10 K, and thus impacts would contribute negligibly to the thermal evolution of a parent body. However, some investigators still argued for evidence of significant impact heating in different chondritic samples, and suggested that porous planetesimals may have been heated to greater levels than seen in these numerical simulations (e.g., Rubin and Jones 2003; Rubin 2004). The role of impact heating was revisited by Davison et al. (2010), who showed that because early planetesimals probably had significant porosity (Blum and Wurm 2008; Cuzzi et al. 2008; Bland et al. 2011), collisions would have produced higher temperatures than previously realized. However, as impact heating is localized and can only affect a small volume of the target planetesimal around the point of impact, the calculations of Davison et al. (2010) showed that the globally averaged temperature increase was only slightly greater than the 10 K increase suggested by Keil et al. (1997), even when we account for the effect of porosity.

In this paper, we quantitatively explore the effects of impacts on the global-scale thermal evolution of a meteorite parent body in the very early solar system. We examine the thermal effects of an impact on a cold (unheated or cooled) parent body in isolation, as well as the thermal effects of impacts on bodies heated by the decay of SLRs, at different stages of their thermal evolution. In each case, we compare the thermal evolution of the impacted planetesimal with the thermal evolution of a planetesimal affected by radiogenic heating alone. We focus here on undifferentiated bodies for the sake of simplicity, although we do use our results to draw inferences about the implications for differentiated meteorite parent bodies. In the next section, we describe the approach and numerical models used in our study. We then examine how the thermal evolution due to impacts involving cold bodies would compare with the thermal evolution in bodies heated by SLRs alone. In the following sections, we explore how an impact into a very early, warm parent body altered the thermal evolution of materials in the planetesimal. We end with a discussion of the implication of our results.

## APPROACH AND MODELS USED

To understand the thermal processing of materials in a realistic planetesimal setting, we must quantify the

thermal evolution of every point in the planetesimal before, during, and after the impact event. We do this using a series of models for each time period and then splice together the thermal histories to determine the overall temperature–time ( $T-t$ ) history of every point in the target body. We then compare the overall thermal evolution of each location to what the  $T-t$  history would have been in the absence of any impact event. Below, we describe the models and techniques used in making this comparison.

While planetesimals would have come in a range of sizes, compositions, and accretion times, we focus here on bodies that are similar to what has been inferred for the H chondrite parent body because its thermal evolution has been considered in detail by previous workers (e.g., Taylor et al. 1987; Trieloff et al. 2003; Kleine et al. 2008; Harrison and Grimm 2010) and allows for detailed comparisons of model predictions to actual meteoritic data. That is, we consider a target 200 km in diameter that accretes instantaneously 2.2 Myr after CAI formation. We extend the results of our study to parent bodies of different sizes and accretion times in the Discussion section.

In all cases, we began with a spherical planetesimal that accreted instantaneously, such that all materials it contained began at the same temperature. We used the 2-D, finite-volume thermal model described in Davison et al. (2012a) to calculate how the heat generated by the decay of  $^{26}\text{Al}$  was produced, redistributed, and radiated away to space from the surface of the planetesimal. This model solves the two-dimensional heat equation in cylindrical coordinates:

$$\rho C_p \frac{\partial T}{\partial t} = \frac{1}{r} \frac{\partial}{\partial r} \left( \rho C_p \kappa \frac{\partial T}{\partial r} \right) + \frac{\partial}{\partial z} \left( \rho C_p \kappa \frac{\partial T}{\partial z} \right) + A_0(r, t) \quad (1)$$

where  $\rho$  is the density of the material in the planetesimal,  $C_p$  is the heat capacity of the material, and  $\kappa$  is the thermal diffusivity of that material. The equations are solved explicitly with a fixed timestep of 1–10 yr (each of which is less than 0.1% of the Courant timestep,  $\Delta t < \frac{(\Delta r)^2}{2\kappa}$ , where we use equal spacings in the  $r$  and  $z$  directions so that  $\Delta r = \Delta z$ ). This model had been previously tested against analytic solutions to the heat equation (Carslaw and Jäger 1959) and shown to produce temperatures that agree through all times within 1% (Davison et al. 2012a). In our models, the spatial resolution is chosen such that  $\Delta r = \Delta z = 500$  m. Simulations with grids half this size were also run and found to produce similar results. We chose this coarser resolution to maintain easy handling between the thermal models and impact simulations, which used the same resolution, and to keep computational run times to a reasonable time period.

Within the literature, a range of values are used for the key parameters in the thermal models for chondritic planetesimals (Yomogida and Matsui 1984; Bennett and McSween 1996; Ghosh and McSween 1999; Elkins-Tanton et al. 2011). Here, we adopt constant values of density  $\rho = 3.32 \text{ g cm}^{-3}$ , heat capacity  $C_p = 8 \times 10^6 \text{ erg g}^{-1} \text{ K}^{-1}$ , and thermal diffusivity  $\kappa = 7 \times 10^{-3} \text{ cm}^2 \text{ s}^{-1}$ , which fall within the range of values used by previous workers. Together, these give a thermal conductivity,  $K = \rho C_p \kappa = 1.86 \times 10^5 \text{ erg cm}^{-1} \text{ K}^{-1} \text{ s}^{-1}$ , which is the value measured for H chondrite meteorite samples by Opeil et al. (2010). As with previous studies, the results of our models will vary in detail with the choice of parameters; however, the key results and broad conclusions we reach will hold regardless of the values.

Using this model, we define a time of accretion,  $t_{\text{acc}}$ , for the planetesimal, which sets the amount of live  $^{26}\text{Al}$  contained within. We assume that the initial abundance of  $^{26}\text{Al}$  in the solar system at  $t = 0$  yields a  $^{26}\text{Al}/^{27}\text{Al}$  ratio of  $5.2 \times 10^{-5}$  (Jacobsen et al. 2008). Thus, at  $t = t_{\text{acc}}$ , the ratio will be  $5.2 \times 10^{-5} \exp(-\lambda t_{\text{acc}})$ , where  $\lambda = 9.5 \times 10^{-7} \text{ yr}^{-1}$  is the decay constant for  $^{26}\text{Al}$ . This means that the  $^{26}\text{Al}/^{27}\text{Al}$  of materials in the planetesimal is  $6.4 \times 10^{-6}$ . The abundance of all Al in the planetesimal is taken to be  $0.0117 \text{ g g}^{-1}$ , which is the value found in H chondrites (Harrison and Grimm 2010). For our purposes, we assume that the 100 km radius parent body accretes at 2.2 Myr, which allows materials to thermally evolve in a manner that is consistent with the thermochronometry of most H chondrites (Harrison and Grimm 2010). We assume an ambient temperature of 170 K throughout our simulation, although the ambient temperature has little effect on our results.

We then model the impact of a planetesimal into the target using the iSALE shock physics code (Wünnemann et al. 2006), an extension of the SALE hydrocode (Amsden et al. 1980). To simulate impact processes in solid materials, several modifications were made to the original SALE code (e.g., Melosh et al. 1992; Ivanov et al. 1997; Collins et al. 2004, 2011a; Wünnemann et al. 2006). iSALE has been extensively validated against laboratory experiments and other hydrocodes (e.g., Pierazzo et al. 2008). It has previously been used to simulate collisions between porous planetesimals (Davison et al. 2010, 2012a). The target body is assumed to have an internal temperature gradient at the time of impact as determined by our radiogenic heating model. The impactor, for simplicity, is assumed to be at a uniform temperature of 170 K. As our interest is on the thermal evolution of the target body, the temperature of the impacting body is found to have a minimal effect on our final results. As in previous studies (Davison et al. 2010, 2012a), we use the

ANEOS equation of state (EOS) for dunite (Benz et al. 1989) to describe the thermodynamic response of the target materials to shock processing and a porosity of 6% in agreement with what has been estimated by Harrison and Grimm (2010) for the H chondrite parent body. Pore space compaction was simulated using the  $\varepsilon$ - $\alpha$  porous compaction model (Wünnemann et al. 2006; Collins et al. 2011a). Based on previous studies (e.g., Wünnemann et al. 2008; Davison et al. 2010), the parameter  $\kappa$ , which controls the rate at which pore space is compacted under compression, was set to 0.98. The target material was assigned a shear strength using the procedure outlined in Collins et al. (2004), with strength parameters for weak rock (Leinhardt and Stewart 2009).

To simulate the entire impact event, including the collapse of the transient crater due to gravity, a self-gravity algorithm was employed (Collins et al. 2011b). This algorithm was based on that described by Barnes and Hut (1986), and has previously been tested against benchmark problems described by Crawford (2010) and used in simulations of planetesimal collisions by Davison et al. (2012b).

Numerical models of large impact events, in which a complex crater is formed, rely on the use of an acoustic fluidization model (Melosh 1979, 1983) to weaken the strength of the target and facilitate wholesale crater collapse, although such processes seem to be much less important during the formation of simple craters. The simple-to-complex crater transition diameter,  $d_{\text{sc}}$ , scales with the inverse power of surface gravity,  $g$  (e.g., Melosh and Ivanov 1999). Taking  $d_{\text{sc}}$  of 18 km on the Moon and  $g = 1.63$  and  $0.087 \text{ m s}^{-2}$  for the Moon and our target body, respectively, we estimate that on our 100 km radius parent body,  $d_{\text{sc}} \approx 300 \text{ km}$ . As this transition diameter is larger than the largest crater that we simulate in this work, we have omitted any acoustic fluidization in the impact modeling for simplicity. To extend the results of this work to larger parent bodies or larger, complex impact craters on this parent body, the effects of acoustic fluidization would need to be considered.

In most of the simulations discussed in this work (those with an impactor radius of 10 km), the resolution was set to a grid size of 500 m per computational cell, in both the  $r$  and  $z$  dimensions. This translated to 20 cells across the impactor radius, and 200 cells across the target body radius. In the simulations with an impactor radius of 4.6 km, the cell size was set to approximately 230 m, to keep the same 20 cells per impactor radius. In this case, the target body had 431 cells across its radius.

All impacts discussed in this work occur at a velocity of  $4 \text{ km s}^{-1}$ . While a large range of impact

velocities was possible in the early solar system (Davison et al. 2013), this represents a typical value for what is expected during planet formation. Here, we only consider vertical incidence impacts, which deposit the maximum amount of heat for a given set of impact parameters. This treatment is adopted in this study to simplify the simulations of both the impact and the thermal evolution, allowing the model to take advantage of cylindrical symmetry, and thus reduce the computational expense and run time. In reality, most impacts would occur at oblique incidence angles, with the most common impact angle being  $45^\circ$  (Shoemaker 1962); changing both the impact angle and the impact velocity can affect the amount of mass heated in a planetesimal collision (e.g., Davison et al. 2012b) and will be quantitatively investigated further in a future publication.

All planetesimals, including meteorite parent bodies, experienced a wide variety of impacts during their early evolution; a 200 km diameter body probably experienced approximately 100–1000 impacts with bodies greater than 300 m in diameter in the first 100 Myr of its life (Davison et al. 2013). We do not model each potential impact scenario, but instead quantify the extent to which a small subset of these impacts would have affected the thermal evolution of the parent body. We use these results to extend the implications to all impacts in the Discussion section further, below.

The impact simulations were deemed to be complete after the crater stopped growing and collapsed under gravity. After all material motions ceased, the postimpact thermal structure of the planetesimal was mapped from the impact model to the same finite-volume thermal evolution code used to calculate the preimpact thermal structure of the planetesimal. The subsequent thermal evolution was then calculated, allowing for loss of preimpact thermal energy, impact-deposited heat, and the generation of any heat produced from the subsequent decay of  $^{26}\text{Al}$ . The thermal evolution is calculated for 200 Myr after the impact.

To quantify the extent that materials in the planetesimal had their thermal evolution perturbed by the impact, we took advantage of iSALE's Lagrangian tracer particles to determine where material that originated at one particular location in the target planetesimal was translated to in the postimpact planetesimal; that is, we recorded both the initial, preimpact  $(r_0, z_0)$  coordinates and the final  $(r_f, z_f)$  coordinates of the tracers in the planetesimal. With this information, we then splice the thermal evolution together for each tracer particle with the thermal evolution at  $t < t_{\text{imp}}$  given by the grid cell that contained the tracer in the spherical, preimpact

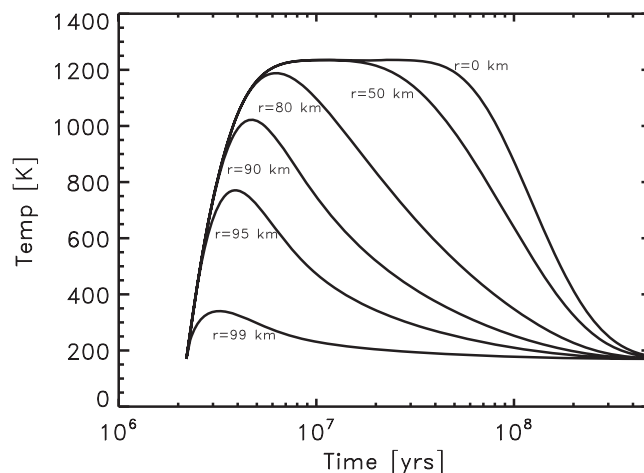


Fig. 1. Temperature–time ( $T-t$ ) evolution of various radial locations in an unimpacted planetesimal as it is heated by the decay of  $^{26}\text{Al}$  as described in the text. Thermal profiles are labeled with their location as measured from the center of the planetesimal. Note,  $t = 0$  here corresponds to the formation of CAIs. The planetesimal is assumed to format  $t = 2.2$  Myr.

planetesimal and the thermal evolution at  $t > t_{\text{imp}}$  given by the grid cell that contained the tracer in the postimpact planetesimal. This ( $T-t$ ) history can then be directly compared with the thermal evolution that tracer would have experienced if the collision had never occurred and it remained in its original grid cell.

### ONION-SHELL THERMAL EVOLUTION

Figure 1 shows the thermal histories of materials at different depths of a spherical planetesimal that does not experience any impact events throughout its evolution and is similar to the results of previous radiogenic heating models (e.g., Tieloff et al. 2003; Kleine et al. 2008; Harrison and Grimm 2010; Henke et al. 2012). An onion-shell structure is apparent in these figures, as the thermal evolution of materials varies with radius. Materials at shallow depths are not significantly warmed as a result of radiogenic heating because the thermal energy produced by radioactive decay is quickly conducted to the surface and radiated away to space. Materials deep inside the planetesimal, on the other hand, reach higher temperatures, as the heat produced from radioactive decay takes longer to diffuse to the planetesimal surface. For these same reasons, there is also an inverse correlation between cooling rates and peak temperatures: material heated to a higher temperature cools more slowly than material heated to a lower temperature.

The petrologic type of a chondritic meteorite indicates the level of thermal processing that the

materials it contains experienced. Models typically define petrologic type based on peak temperature, without regard to time spent at that temperature. Thus, if we adopt the categories defined by Harrison and Grimm (2010), type 6 meteorites ( $T_{\text{peak}} = 1138\text{--}1273\text{ K}$ ) would come from inside  $r < 84\text{ km}$  (where we have defined  $r = 0$  as the center of the planetesimal), type 4 and type 5 meteorites ( $T_{\text{peak}} = 948\text{--}1138\text{ K}$ ) would come from  $84\text{ km} < r < 91\text{ km}$ , and type 3 meteorites ( $T_{\text{peak}} < 948\text{ K}$ ) would come from  $r > 91\text{ km}$  in the parent body considered here. As discussed above, the detailed location for each petrologic type depends on the assumed thermal parameters and time of accretion in the model; for example, Harrison and Grimm (2010), who used parameter values that provided the best match of their model predictions to H chondrite data, predicted that the petrologic types 6, 4-5, and 3 would come from  $r < 88\text{ km}$ ,  $88\text{ km} < r < 99\text{ km}$ , and  $r > 99\text{ km}$ , respectively. The differences in estimated depth in the model used here and those in Harrison and Grimm (2010) stem from the different thermal diffusivities, heat capacities, and densities assumed in the model. The initial structure is important in estimating the amount of mass whose petrologic type changes as a result of impact. We note that our thermal model predicts lower near-surface temperatures than the model of Harrison and Grimm (2010). As most impact heat is deposited at the surface of the target planetesimal, our results probably overestimate the mass of material whose petrologic type changes due to impact than would be found using the structure given by Harrison and Grimm (2010).

### THERMAL CONSEQUENCES OF A LATE IMPACT

Figure 2 shows the postimpact thermal structure of a cold target body—that is, one that was never heated by radioactive decay or one that had lost all of its radiogenic heat—after experiencing a collision with a 10 km impactor at  $4\text{ km s}^{-1}$ , at a vertical incidence impact angle. Such a collision has approximately 1% of the energy necessary to disrupt the target planetesimal, a value comparable to the most energetic impact experienced by most surviving 100 km radius parent bodies over the course of their evolution (Davison et al. 2013). That is, on average, every 100 km radius parent body that survived beyond 100 Myr without being collisionally disrupted would have experienced an impact with this energy over this early time period. While more energetic impacts could have occurred, they would have been much less common, and may have led to disruption. As such, we focus on the most common, “most energetic” impact that a body of this type would have experienced in the early solar system.

The left-hand side of Fig. 2 shows the growth the crater during this impact. In the top frame, the initial conditions of the model are shown, at the point of contact between the impactor and target bodies. After 750 s, the transient crater has formed with a radius of around 70 km. The frame at 3500 s shows material slumping back into the center of the crater, and burying the heated material beneath the center. By 8500 s, all material motions have stopped. The final crater has a radius of around 90 km (approximately equal to the radius of the target body). Most of the heat deposited in the collision lies within an approximately 30 km region beneath the center of the crater (Fig. 2).

While the amount of heating that occurs in such collisions has been considered in previous studies (Keil et al. 1997; Davison et al. 2010, 2012a), here we consider how the postimpact thermal evolution differs from that from radioactive decay alone. We assume that the impact occurred 500 Myr after the planetesimal formed, a time by which the planetesimal lost all radiogenic heat. The heat from the impact is then redistributed as a result of conduction through the planetesimal and radiative loss from the surface to space. Note, we ignore any additional heat input from radionuclides, both short-lived (which would be extinct at this point anyway) and long-lived.

The thermal profiles of materials at different depths in the planetesimal are shown in Fig. 3. We focus on the thermal evolution of materials at the same preimpact depths as those materials shown in Fig. 1, measured along the line connecting the center of the target and the point of impact. While the planetesimal experiences its expected onion-shell thermal evolution prior to impact, points in the planetesimal become perturbed by the impact at later times. In some cases, materials reach higher postimpact temperatures than achieved from radiogenic heating alone. For example, the materials buried approximately 1 km below the surface in our onion-shell model reach a peak temperature of approximately 340 K as a result of SLR heating, but reach temperatures of 785 K as a result of impact heating. At a depth of 5 km, SLR heating and impact heating both produce peak temperatures of approximately 770 K. At greater depths, postimpact temperatures are significantly less than those produced during onion-shell evolution; at 10 km, the impact heats materials to temperatures of approximately 500 K, compared to the approximately 1020 K reached by SLR heating.

Figure 4 shows how the late impact perturbs the onion-shell thermal histories of different regions of the planetesimal, by plotting the thermal record of each tracer in the radiogenically heated and then impacted planetesimal versus what would be recorded in a

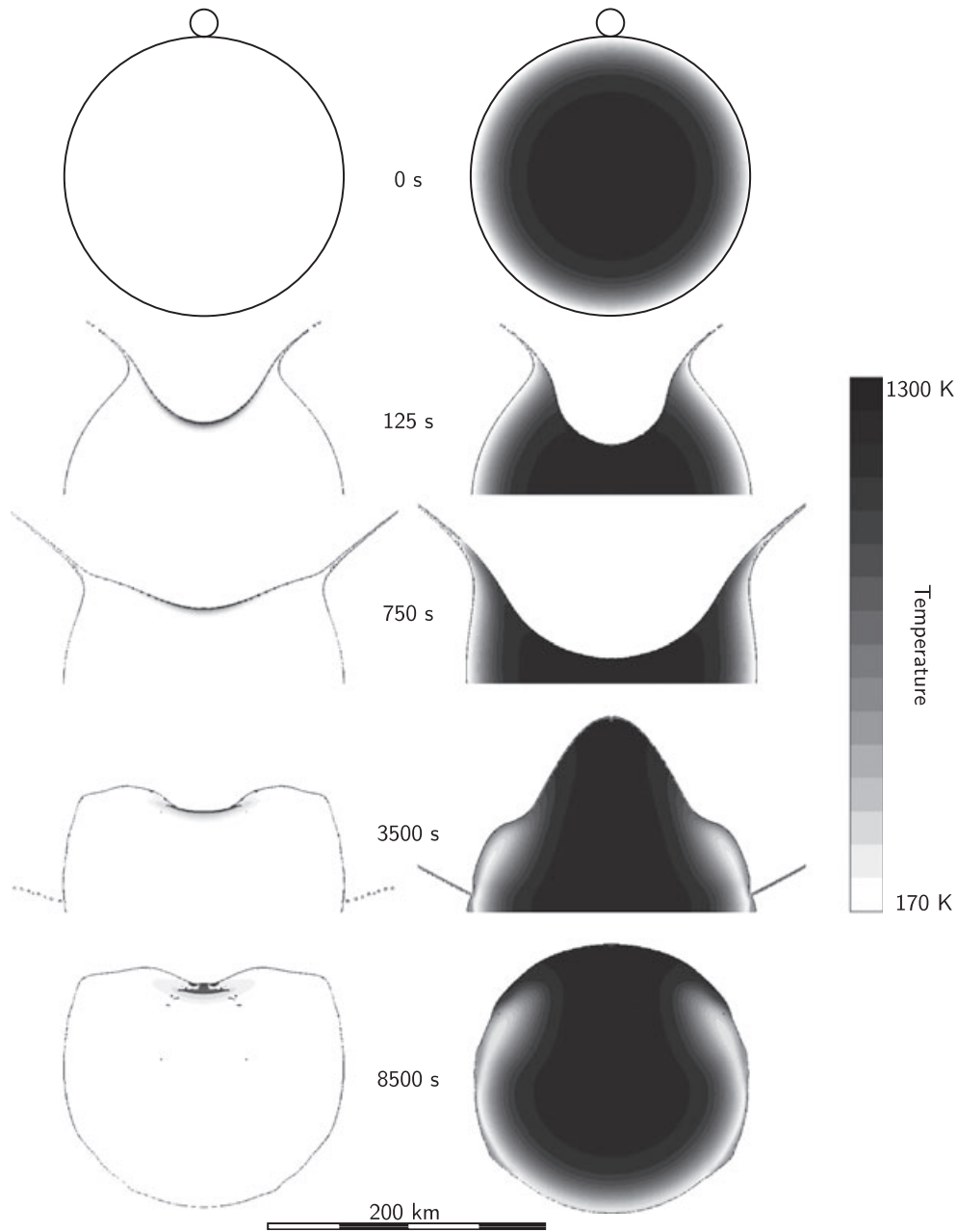


Fig. 2. Crater formation in the impact into a cold target body (left) and the impact at 10 Myr (right). Times indicate the time after impact. The transient crater has formed in both cases at around 750 s. At 3500 s in the cold case, material has begun collapsing toward the crater center, but in the impact at 10 Myr, a large central uplift has formed: This frame shows it at its maximum height. By 8500 s, all material motions have stopped, and the final structure is ready to be passed back to the thermal evolution code.

planetesimal heated by SLRs alone (note, due to the cylindrical coordinate system used here, not every point represents the same amount of mass). Specifically, we focus on the peak temperature reached ( $T_{\text{peak}}$ ) and the cooling rate, which is the rate at which the material cooled for the last time through 773 K (500 °C), the temperature at which metallographic cooling rates are

recorded (Taylor et al. 1987; Harrison and Grimm 2010).

While some heat was deposited in the target planetesimal during impact, only a small fraction of mass reached temperatures in excess of those reached during radiogenic heating. This extreme impact heating was confined to an area around the point of

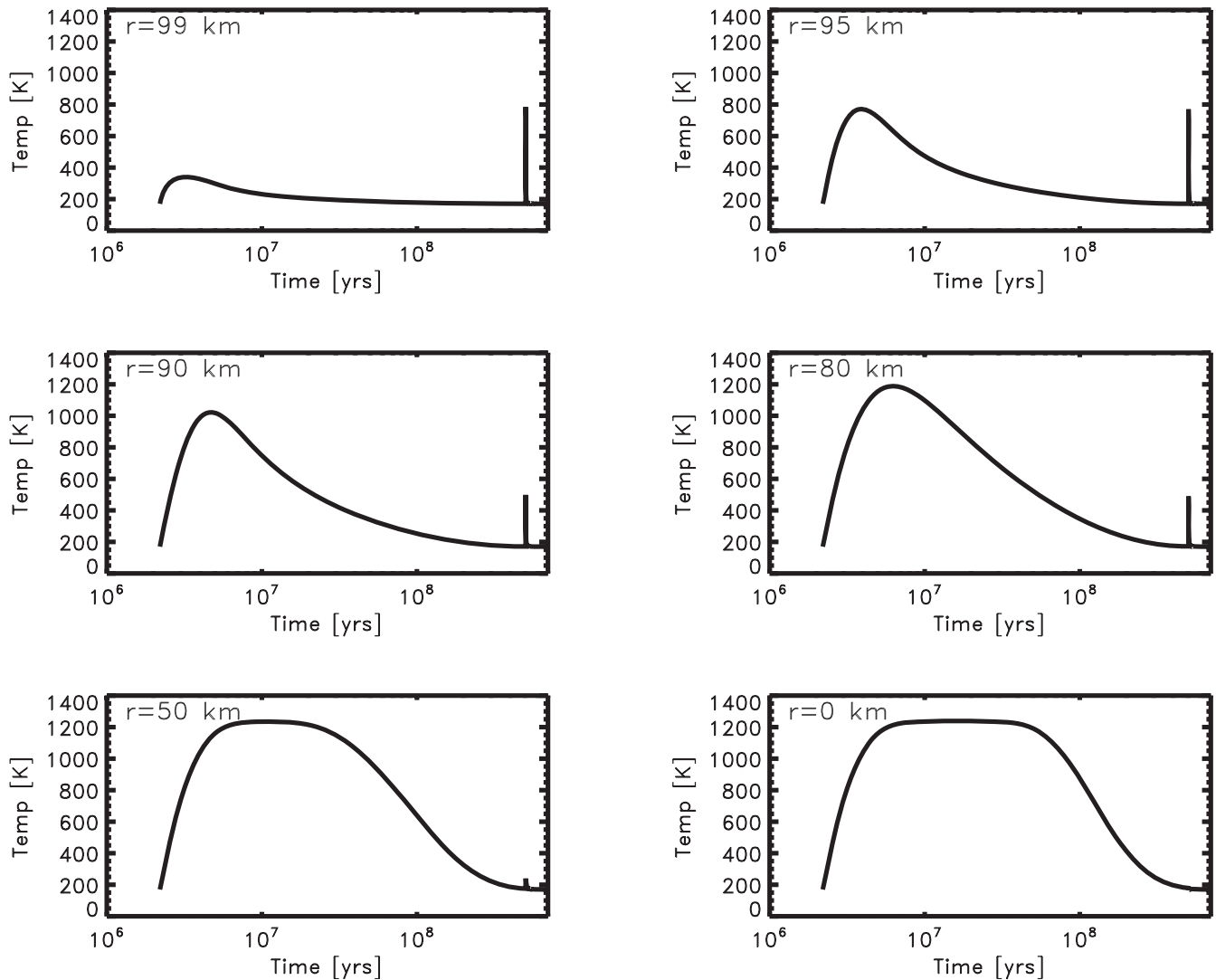


Fig. 3.  $T$ - $t$  histories of the same points shown in Fig. 1 in a planetesimal that is impacted 500 Myr after its formation. Locations corresponded to the depth in the preimpact body along the line connecting the planetesimal center and the point of impact. Note, the temperature spikes near the surface of the planetesimal allow the materials to reach higher temperatures than achieved from  $^{26}\text{Al}$  alone.

impact, less than approximately 5 km deep as shown in Fig. 3. This heated mass corresponds to those tracers that plot above a one-to-one line in the left panel of Fig. 4. To assess the extent to which impact heating was sufficient to induce changes in petrologic type, we can identify regions of the planetesimal where impact-induced peak temperatures would change (raise) the petrologic classification from its classification based on a radiogenic heating model alone. If we assume that the thermal alteration in a meteorite is determined purely by the peak temperature, without regard for time spent at that temperature, as is done in radiogenic models (Trieloff et al. 2003; Kleine et al. 2008; Harrison and Grimm 2010), then  $5.8 \times 10^{14}$  kg ( $4.2 \times 10^{-5}$  of the mass of

the target) would be transformed to higher petrologic types by the impact.

Resetting of metallographic cooling rates—that is, reheating materials above 773 K and then allowing them to cool below that temperature at a different rate—occurs in a slightly greater portion of the target,  $1.8 \times 10^{15}$  kg or  $1.3 \times 10^{-4}$  of the total body, with most of this reset mass being found in the outer edge of the planetesimal near the point of impact. In radiogenic models, the outer portion of the target may record no cooling rate, as it never reached temperatures in excess of 773 K. Thus, much of the material around the point of impact would never have been heated to such levels without the impact, but is now able to record a cooling rate even if it does not change its petrologic type.

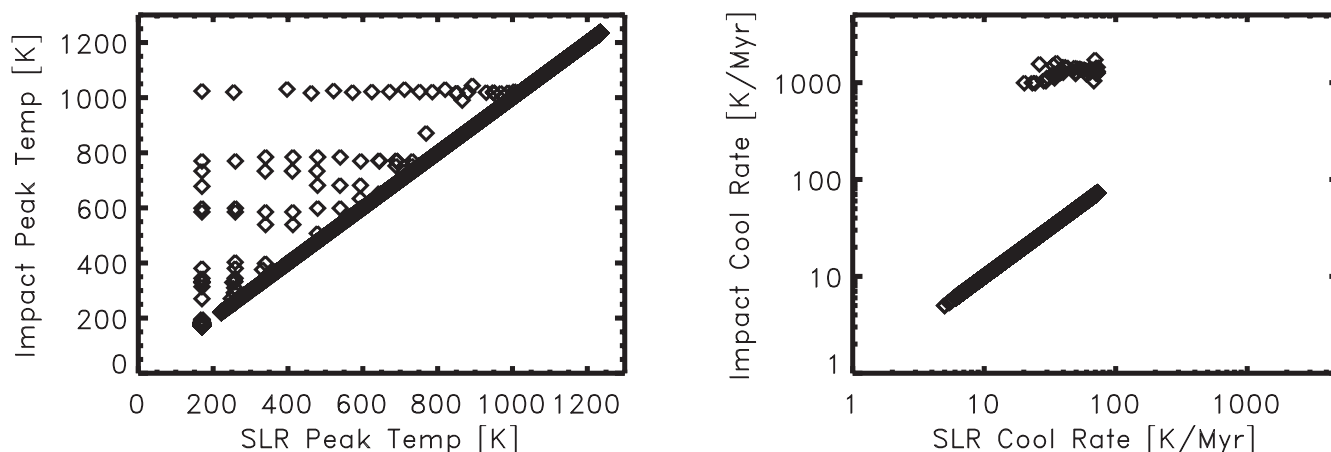


Fig. 4. Left) Plot of peak temperature reached by tracers in the impacted planetesimal in Figs. 2 and 3 accounting for heat from both short-lived radionuclides (SLR) and impacts versus what they would be in the unimpacted planetesimal from SLR alone. Right) Plot of the cooling rate at 773 K experienced in the impacted planetesimal versus what it would be in the unimpacted planetesimal. In both plots, materials unaffected by the impact plot on the slope 1 line, whereas the materials disturbed by the impact plot above the line (having experienced higher peak temperatures and faster cooling rates).

In total, these results are in agreement with the general conclusions of Keil et al. (1997) that any significant increases in temperature due to planetesimal collisions would be negligible on the global scale. However, localized temperature perturbations can be significant and cooling rates that develop may be comparable to those seen in chondritic meteorites (Davison et al. 2012a).

### IMPACTS INTO RADIOGENICALLY HEATED PLANETESIMALS

The scenario envisioned in the previous section, a collision between two uniformly cold bodies, would only have occurred in our solar system many hundreds of millions of years after the parent bodies formed. That is, radiogenic heat persisted in such bodies for 0.1–1 Gyr, depending on the time of formation and size of the body. However, models for the evolution of the asteroid belt find that in a primordial asteroid belt significantly more massive than found today, the current size distribution of bodies was achieved after approximately 500 Myr of collisional grinding (O'Brien and Sykes 2011). That is, bodies experienced frequent collisions immediately after their formation, when the mass of the asteroid belt exceeded its current value by orders of magnitude. In fact, in the models of O'Brien and Sykes (2011), the frequency of collisions is expected to have been much greater in the first 500 Myr than even during the Late Heavy Bombardment period of solar system history, owing to the larger number of bodies present during the formation of the planets. Even in a dynamic environment like that predicted by the Grand Tack (Walsh et al. 2011), the larger numbers

of bodies present during planet formation suggest that collisions would have been more frequent during the early stages of planet formation, even if the asteroid belt was not many orders of magnitude more massive than today.

Collision rates among asteroids are found to be highest in the first approximately 100 Myr, with a peak occurring some 5–20 Myr into solar system history (Davison et al. 2013). This is important as this peak collision rate coincides with a time when planetesimals were at or near their peak temperatures as a result of radioactive decay. As target materials will respond to stresses imparted during an impact differently depending on their temperature (an effect known as thermal softening, e.g., Ohnaka 1995; Collins et al. 2004), it is necessary to explore the thermal consequences of impacts at different times during the thermal evolution of the target.

Figure 5 shows the pre- and postimpact thermal structure for impacts into a 100 km asteroid occurring at different times during its early evolution; that is, during the time that its thermal state is evolving as a consequence of heating from  $^{26}\text{Al}$  decay. In each case, the properties of the impactor and target planetesimal are the same as the scenario considered above. The impact processes vary depending on the timing of the impact after formation.<sup>1</sup> When the impact occurs into a relatively cold target, the cratering process is slowed by the high strength of the cool target material, leading to a final crater with some heated material buried under the central debris lens (e.g., the impact at 1 Myr in

<sup>1</sup>An animation for the impact simulations described here can be found at: [http://geosci.uchicago.edu/~fciesla/movies/Heated\\_Impacts.avi](http://geosci.uchicago.edu/~fciesla/movies/Heated_Impacts.avi)

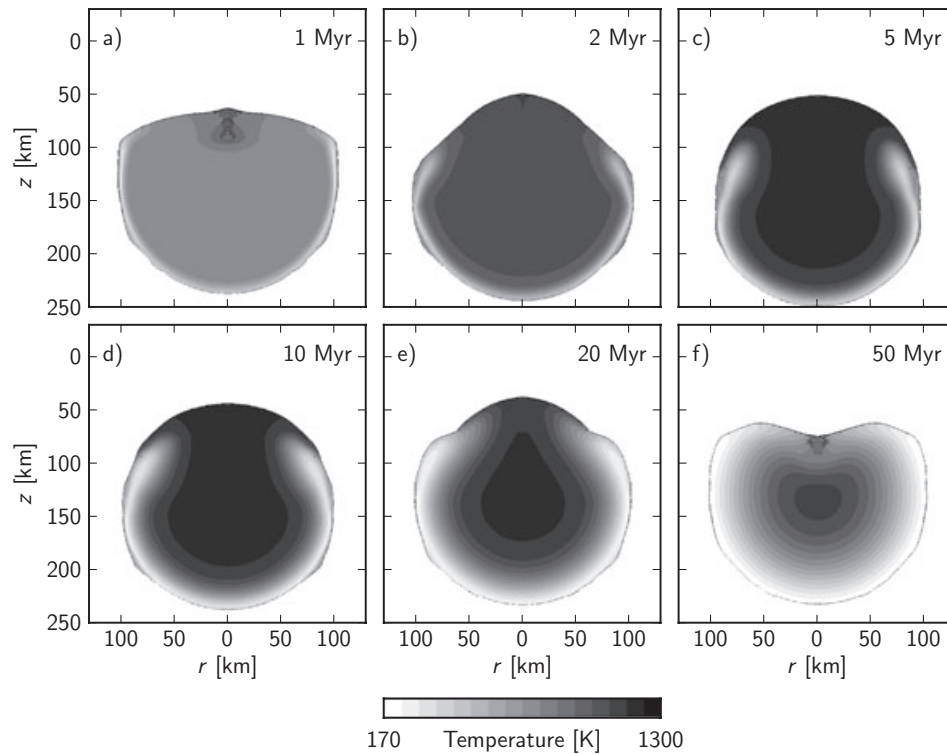
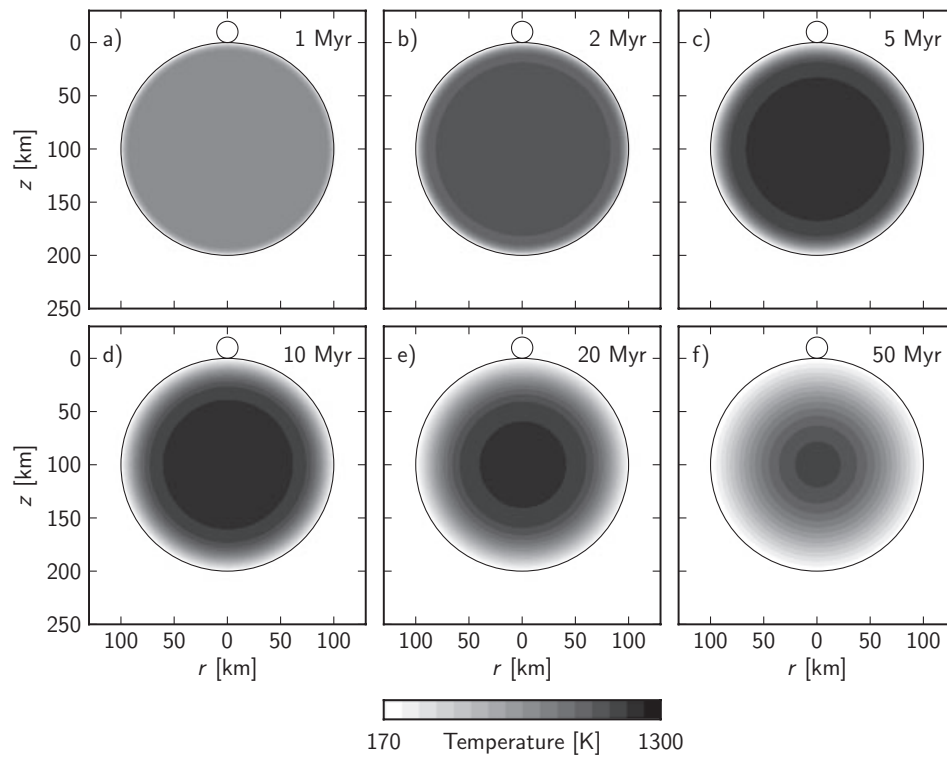


Fig. 5. The pre- (top) and postimpact (bottom) thermal structure of the planetesimal in the simulations described in the text. Impacts are simulated at different times after the formation of the planetesimal, as indicated in each panel. The thermal softening of interior rock plays a major role in determining the postimpact structure of the planetesimal and the distribution of materials heated by the decay of short-lived radionuclides. Thus, the net effect of the impact on the thermal evolution of the planetesimal is strongly dependent on the time of impact.

Fig. 5 and the impact into a cold target discussed above). However, once the target has been heated more strongly (i.e., from 2 Myr onwards), the thermally softened target material flows much more readily. Thus, the opening of a transient crater is halted not by material strength, but by the weight of the material under the gravitational influence of the target body. Moreover, for impacts occurring between 2 and 20 Myr, gravitational collapse of the transient crater results in a large central uplift. In the target body impacted at 2 Myr, at the time of maximum uplift, the diameter of the planetesimal measured along the line connecting the point of impact to the impact antipode through the center of the body is approximately 200 km—that is, the body returns to a near-spherical shape, and then material movements stop. In the planetesimals that are impacted at 5 Myr and 10 Myr, which have a higher initial temperature than at 2 Myr, the central uplift is larger: The maximum dimension of the planetesimal is approximately 230 km, measured along the line connecting the planetesimal center and point of impact. This means that the central uplift then relaxes under gravity as it returns to a near-spherical geometry. As a result, some hot material flows over the surface of the planetesimal away from the center of the impact, leading to burial of some cooler material located near the surface before the impact. The cratering formation in the planetesimal impacted at 10 Myr is shown on the right-hand side of Fig. 2. Compared with the impact crater formed in a cold body, the transient crater is deeper (see the image at 750 s after impact). At 3500 s, the maximum extent of the central uplift can be seen. By 8500 s, the central uplift has collapsed, and the planetesimal has returned to a near-spherical shape, with some hot material from deep inside the planetesimal flowing out over cooler material from near the preimpact surface. By 20 Myr, the target body had cooled to the point that the effect of the central uplift and increased material flow is diminished. In this case, the maximum extent of the body is approximately 210 km, and thus burial of the cooler outer layers by outward collapsing hot rocks from the central uplift is less extensive at this time. By 50 Myr, the outer layers of the planetesimal have cooled to the point that their high initial strength has returned. As a consequence, no central floor uplift occurs, and the final form of the crater resembles that of the crater formed on a cold, unheated planetesimal (i.e., at 500 Myr or at 1 Myr).

We note here that while it has been suggested that planetesimals may become strengthened or experience porosity loss due to sintering at high temperatures (Hevey and Sanders 2006; Sahijpal et al. 2007), we ignore any changes to material properties due to cycling to high temperatures and cooling again.

To identify the key differences between impact into a hot body and impact into a cold body, we examine the thermal consequences of the  $t_{\text{imp}} = 10$  Myr impact and compare these in detail with the consequences of impact into the cold (unheated or completely cooled) planetesimal. This time period was chosen as it corresponds to the peak in the impactor flux of the early solar system in the models of Davison et al. (2013). In the next section, we discuss how results vary depending on the time of the impact.

Figure 6 compares the pre- and postimpact positions of all retained tracers in the target planetesimals for a uniform temperature, cold (170 K) target and one that was impacted 10 Myr after its formation (maximum internal temperature approximately 1235 K). Tracers were placed within the center of each grid cell at the beginning of the impact simulations and the position, temperature, and pressure that their corresponding mass elements experienced throughout the impact simulation were recorded. The tracers in Fig. 6 are shaded according to their original location in the planetesimal, divided into 10 different bands, each representing a spherical shell 10 km thick. Absent tracers in the outer 10 km shells represent mass ejected from the planetesimal at speeds exceeding escape velocity and hence not present in the postimpact planetesimal. This corresponds to approximately  $1.6 \times 10^{17}$  kg in the cold planetesimal and approximately  $3.9 \times 10^{17}$  kg in the heated planetesimal (approximately 1.2% and 2.9% of the target bodies or  $11\times$  and  $28\times$  the mass of the impactor, respectively). The key difference between impact into a cold and hot target is that materials from the center of the target are displaced much farther in the hot planetesimal than in the cold planetesimal because the hot planetesimal's interior is thermally softened and more ductile. In this particular case, materials originally located nearly 50 km deep (halfway into the planetesimal) were brought to the surface at the impact point. Furthermore, hot ductile material uplifted from 10–30 km depth flowed outwards from the center during relaxation of the central uplift and covered much of the pristine, unheated surface of the planetesimal, except at the antipode of the impact site. This contrasts with the impact into a cold planetesimal, in which the cold, rigid interior structure of the planetesimal is barely disturbed by the impact, with material from no deeper than approximately 10 km below the surface being exposed around the point of impact.

The impact alters the subsequent thermal evolution of the hot planetesimal in a variety of ways. Figure 7 shows how the temperature of material at different locations is affected by the impact. Each curve shows the  $T$ - $t$  record of material originating from the equivalent location in the planetesimal to those points

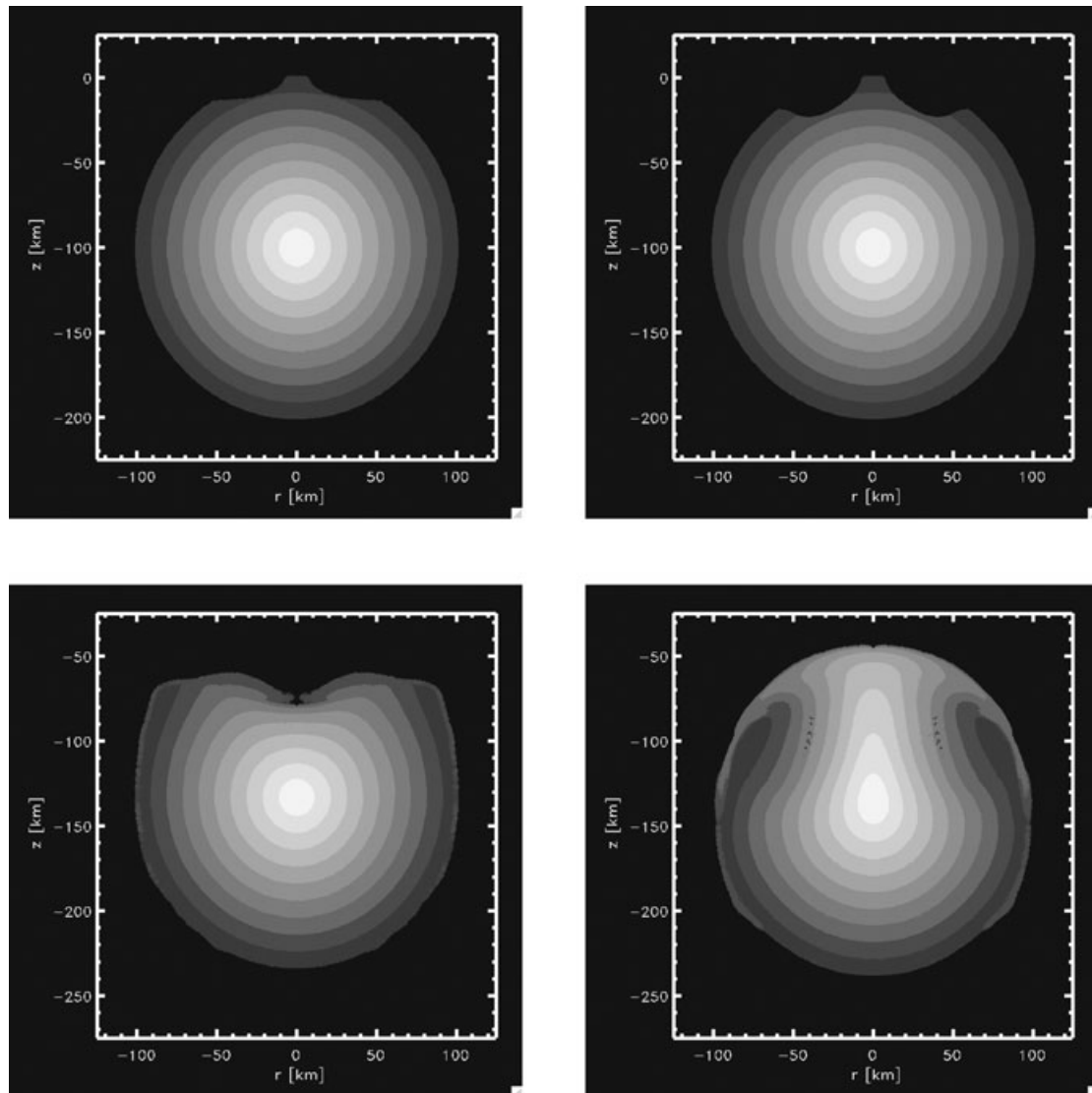


Fig. 6. Top panels show the preimpact positions of the target tracers, which remain in the planetesimal after the collision, while the bottom panels show the postimpact positions. Note, tracers are color coded by their initial depth in the planetesimal. Left panels are for the case of a uniformly cold planetesimal expected some approximately 500 Myr after accretion when all radiogenic heating is lost. Right panels are for the case of an impact that occurs 10 Myr after the accretion of the planetesimal. Note how the thermal softening in the target 10 Myr after its accretion allows materials from the deep interior to be brought to the surface as a result of the impact.

shown in Figs. 1 and 3. The perturbation from the impact is severe at most of these locations, with the thermal evolution changing drastically as deep as 50 km from the point of impact, while any change at the center of the planetesimal is negligible. One obvious effect of the impact is that some portions of the target body are shock heated to higher temperatures. This effect is limited to material proximal to the impact site. Again, we can consider the fraction of the planetesimal heated by the impact to a temperature that would cause it to be classified as a higher petrologic type than would be the case if it remained in an unimpacted body.

Figure 8 shows the pre- and postimpact locations of the tracers in the planetesimal, this time shaded by the petrologic type assigned to them as a result of their complete (pre- and postimpact) thermal evolution. In the preimpact plots, one readily sees the onion-shell structure with type 6 materials being found in the interior, type 4/5 materials occupying a spherical shell approximately 7 km thick, and type 3 materials occupying the outermost shell. The only exception to this pattern is at the point of impact, where the type 3 and type 4/5 materials are shock heated to temperatures in excess of 1138 K, and thus become type 6 materials

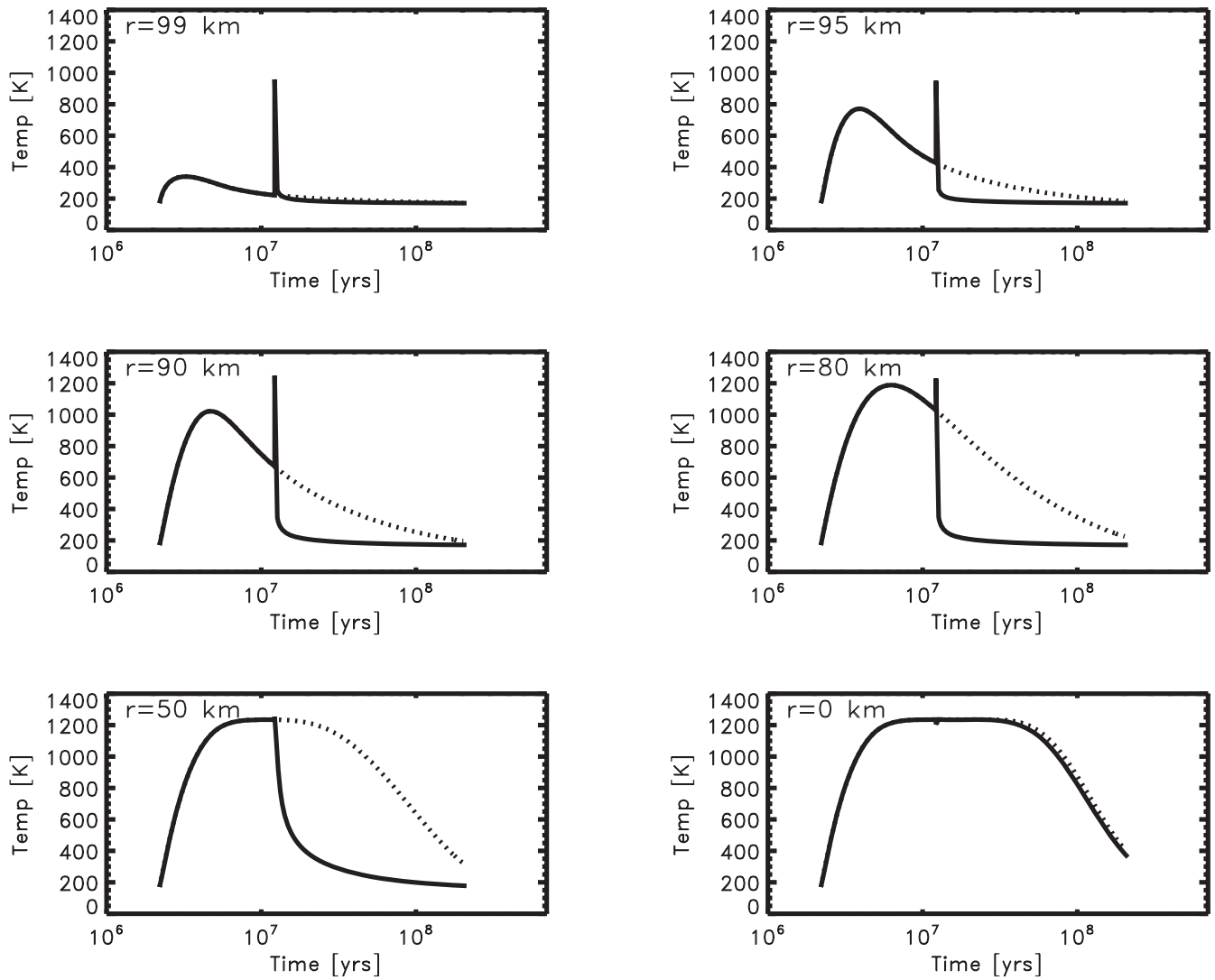


Fig. 7.  $T-t$  histories of the same points illustrated in Figs. 1 and 3 for the case of an impact occurring 10 Myr after the formation of the target body. The heating caused by the impact is seen by the spike occurring at 12.2 Myr after CAI formation in each thermal profile. Furthermore, the increased cooling rate is also readily seen by the dramatic increase in the magnitude of the slope that occurs following the impact event.

(note, no tracers recorded temperatures  $>1273$  K, and thus all material remained below the solidus temperature of our proxy planetesimal material throughout the simulation). The total mass of material that is shock heated to the point that its petrologic type differs from what it would have been in an onion-shell planetesimal is  $9.1 \times 10^{15}$  kg, or 0.07% of the target planetesimal. Thus, again, shock heating only has an effect immediately around the point of impact, and is negligible on the global scale.

Shock heating is not the only means by which target materials achieve higher temperatures as a result of the impact. The burial of otherwise pristine crustal rock by hot material exhumed from depth heats the buried rock to higher temperatures than it would

otherwise achieve. This is due to two effects. First, burial means that a given volume is covered by more insulating material, increasing the time scale for its preimpact heat to be conducted to, and radiated away from, the surface. Thus, the rate of energy loss from a newly buried region decreases compared with what it would be in an onion-shell planetesimal. Second, the buried crust is covered by radiogenically heated material, which flowed out from the center of the planetesimal. This provides an additional source of heat for the crustal materials, as heat would be conducted down from this higher-temperature material into the cooler substrate. In this particular case, no materials have their petrologic types changed as a result of this effect, but peak temperatures in some regions do reach

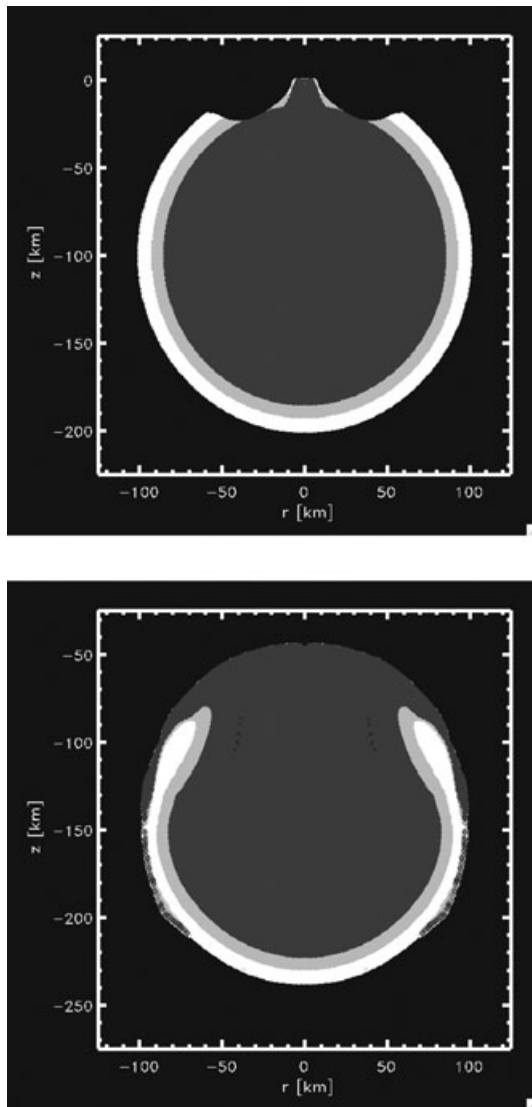


Fig. 8. The pre- (top) and postimpact (bottom) locations of the different petrologic types in the planetesimal, which was impacted 10 Myr after its formation. Type 3 materials are white, type 4/5 light gray, and type 6 are dark gray. The onion-shell structure is apparent in the preimpacted planetesimal, with the only materials deviating from that trend being the type 6 material around the point of impact.

100–200 K above what they would reach in the onion-shell structure.

Thus far, we have focused on the region of the planetesimal that is heated as a result of the impact; this is the primary outcome of an impact that has been invoked to explain features in meteorites in previous studies. While the impact clearly leads to increases in the temperature of some regions of the planetesimal in our simulations, there are other consequences for the subsequent thermal evolution of the body. The upward flow of hot material from the center of the planetesimal

toward the surface allows this material to cool much more rapidly than it would if it remained deep within an undisturbed planetesimal. In fact, cooling rates increase in >50% of the planetesimal as a result of impact. However, for much of this material, the increase in cooling rates may not be sufficient to alter the characteristics of the metal grains contained in a given region. Metallographic cooling rates are uncertain by a factor of approximately 2.5 (Taylor et al. 1987; Harrison and Grimm 2010); thus, slight changes in cooling rates would probably not be detectable in a given meteorite. Figure 9 shows the region of the planetesimal where the cooling rates differ by >2.5 $\times$  what would be reached in the onion-shell planetesimals. This constitutes some 13% of the surviving planetesimal, and includes materials originally located approximately 30 km from the center of the planetesimal, or 70 km below the surface. This mass of material greatly exceeds the mass that increases in petrologic type. Hence, impacts have a much greater influence on global cooling than they do on global heating. Furthermore, the depth to which cooling rates are affected greatly exceeds that predicted by the basic scaling laws used in previous studies (e.g., Harrison and Grimm 2010), which were largely based on cool target bodies.

#### IMPACTS AT OTHER TIMES AND SIZES

In Table 1, we report the fraction of the 100 km radius target whose thermal state is perturbed in various ways as a result of an impact of the type considered above (10 km radius impactor at 4 km s<sup>-1</sup>), but at different times after its formation. Again, we assume that the target body forms instantly 2.2 Myr after CAI formation. The table documents the fraction of the surviving target body that is assigned a different petrologic type to what it would have been assigned in an onion-shell model using the temperature ranges defined in Harrison and Grimm (2010). It also lists the target planetesimal fraction that has a postimpact cooling rate (at the last time it cools below 773 K) that differs from the cooling rate predicted by an onion-shell model by more than a factor of 2.5.

The table shows that regardless of the time of impact, some amount of material is heated to the level that its petrologic type is higher than what it would be in an onion-shell model with no impact. Interestingly, there are portions of the target that reach petrologic types that are below what they would have reached in an onion-shell model in some cases. This is hot planetesimal material uplifted by the impact from deep within the body closer to the surface. Because of its increased proximity to the surface, this material loses

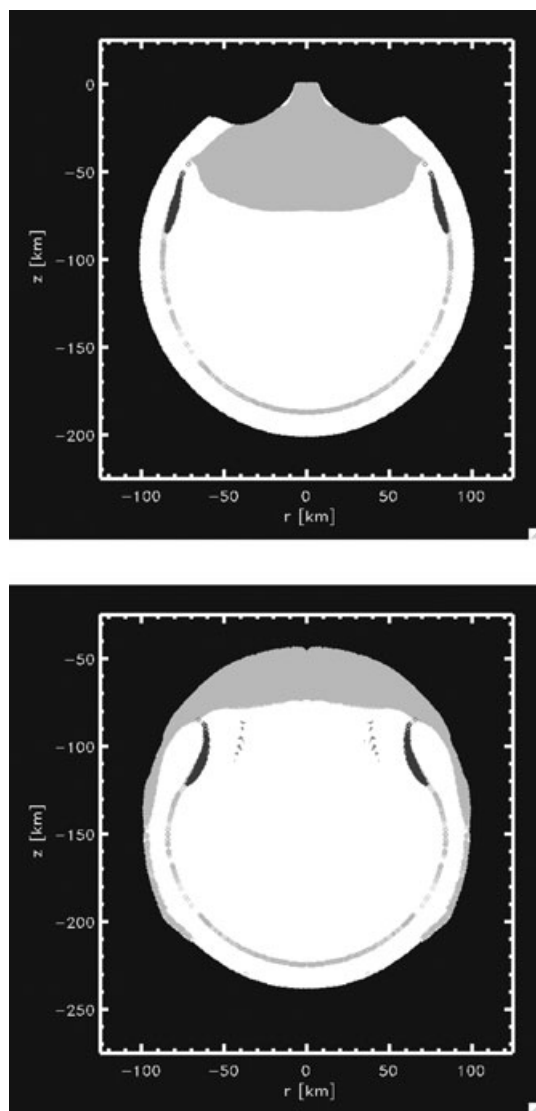


Fig. 9. Pre- (top) and postimpact (bottom) positions of mass in the planetesimal in which the cooling rates at 500 °C of the materials change by more than a factor of 2.5 compared to what they would have been in a pure onion-shell model. Light gray indicates those materials in which the cooling rate increases by at least this amount, while dark gray indicates those materials in which the cooling rate decreases by this amount.

thermal energy from the decay of  $^{26}\text{Al}$  more efficiently and therefore does not reach the same peak temperature it would have reached if it remained deep within the planetesimal, had the impact not occurred. This effect is limited to those impacts that occur early in the history of the planetesimal ( $\leq 5$  Myr) and is not significant at later times, as the peak temperatures of a planetesimal heated by  $^{26}\text{Al}$  are achieved in the first 3–5 Myr of solar system history. After this time period, the input of thermal energy from SLRs becomes negligible and the

body evolves simply by conducting existing heat to the surface where it is radiated away to space.

In all cases, the fraction of the target body that experiences a measurable increase in cooling rate exceeds the mass of the material that has its cooling rate decreased. We specify “measurable increase” here as we focus on those cooling rates where the difference in the cooling rates between those recorded in an unimpacted and impacted onion-shell planetesimal is greater than a factor of 2.5, which is taken as the uncertainty in the reported values from meteoritic studies (e.g., Harrison and Grimm 2010). Thus, these fractions are lower limits as greater mass fractions have their cooling rate altered by smaller factors.

Again, the small amount of mass in the impacted planetesimal that records a cooling rate lower than it would according to the onion-shell model is largely a result of material buried by insulating crater ejecta, trapping heat more efficiently. Increased cooling rates caused by impact arise largely because hot material deep in the onion-shell planetesimal is brought closer to the surface where heat is lost more effectively. In all impact scenarios, the mass fraction with a higher cooling rate than predicted by the onion-shell model exceeds by factors of 10–100 both the mass fraction with a lower cooling rate and the mass fraction with a higher petrologic type than predicted by the onion-shell model. This, combined with the large mass fraction of an impacted planetesimal with a lower petrologic type than predicted by the onion-shell models, suggests that the major effect of impacts in the early solar system was to accelerate the cooling of a body. That is, impacts into bodies heated by radioactive decay in the early solar system aided in the loss of thermal energy more than they contributed to the thermal budget of a body.

We also performed simulations of a smaller, 4.6 km radius impactor colliding at  $4 \text{ km s}^{-1}$  with the same 100 km radius target body considered above, and the results are presented in Table 2. This radius was chosen to provide an impactor mass (and thus impact energy) that was  $10\times$  less than that considered in the previous section. Impacts with this lower energy would be approximately  $10\times$  more common during the first 100 Myr of solar system evolution (Davison et al. 2013). In general, a smaller fraction of the planetesimal mass is affected than in previous cases, with the exception being the amount of mass heated to higher petrologic types in the  $t = 1$  and 2 Myr impacts. This is due to the fact that while the larger impact deposits more heat, it also deforms the target planetesimal to a greater degree. This greater level of deformation increases the surface area-to-volume ratio for the resulting planetesimal (a ratio that is minimized by a spherical planetesimal) and thus greater portions are

Table 1. The fraction of a 100 km radius target body that is “disturbed” by a 10 km radius impactor striking it at  $4 \text{ km s}^{-1}$  at various times after its formation.

Time of impact (years after accretion)	Fraction of target where petrologic type increases	Fraction of target where petrologic type decreases	Fraction of target where cooling rates increase by $>2.5\times$	Fraction of target where cooling rates decrease by $>2.5\times$
1 Myr	0.013	0.083	0.072	0.01
2 Myr	$8.5 \times 10^{-3}$	0.062	0.13	$1.3 \times 10^{-3}$
5 Myr	$6.3 \times 10^{-3}$	–	0.18	0.027
10 Myr	$7.3 \times 10^{-4}$	–	0.13	$7.7 \times 10^{-3}$
20 Myr	$2.8 \times 10^{-4}$	–	0.063	$3.6 \times 10^{-4}$
50 Myr	$3.2 \times 10^{-5}$	–	$8.9 \times 10^{-3}$	$6.3 \times 10^{-5}$
After radiogenic heat is lost ( $>500$ Myr)	$4.2 \times 10^{-5}$	–	$1.3 \times 10^{-4}$	–

Table 2. The fraction of a 100 km radius target body that is “disturbed” by a 4.6 km radius impactor striking it at  $4 \text{ km s}^{-1}$  at various times after its formation.

Time of impact (years after accretion)	Fraction of target where petrologic type increases	Fraction of target where petrologic type decreases	Fraction of target where cooling rates increase by $>2.5\times$	Fraction of target where cooling rates decrease by $>2.5\times$
1 Myr	0.022	$8.28 \times 10^{-3}$	$4.95 \times 10^{-3}$	$3.49 \times 10^{-3}$
2 Myr	0.014	$3.59 \times 10^{-3}$	0.013	$1.3 \times 10^{-5}$
5 Myr	$5.2 \times 10^{-4}$	–	$9.4 \times 10^{-3}$	$2.5 \times 10^{-4}$
10 Myr	$3.6 \times 10^{-5}$	–	$5.4 \times 10^{-3}$	–
20 Myr	$1.2 \times 10^{-6}$	–	$1.9 \times 10^{-3}$	$4.8 \times 10^{-5}$
50 Myr	$1.4 \times 10^{-6}$	–	$8.9 \times 10^{-4}$	–

able to lose heat more readily. This is a minor effect, however, and the same trend is observed for the smaller collision that the redistribution of material by impact into a radiogenically heated body increases the cooling rate of a mass of material that is much greater than the mass that has its petrologic type increased by impact heating.

While we considered only 100 km radius planetesimals here, larger bodies may have been affected to an even greater extent by the same processes, as the number of impacts a target experiences scales with its surface area and because such bodies typically experience even more energetic collisions than considered here (Davison et al. 2013). Furthermore, larger bodies retained their radiogenic heat for longer periods of time, meaning later impacts could accelerate cooling to a greater degree. This would also be important in bodies that accreted earlier, as the greater amount of  $^{26}\text{Al}$  would have led to higher peak temperatures and longer cooling periods in a given target body. In the future, such impact effects should be considered in the thermal histories of large bodies like those proposed for the CV chondrite parent body (Elkins-Tanton et al. 2011; Sahijpal and Gupta 2011), Ceres (Castillo-Rogez and

McCord 2010) or Vesta (Ghosh and McSween 1999) as the long-term processing expected on these bodies would probably be disrupted or disturbed by such impacts. These may be critical to interpreting the histories of these bodies.

## DISCUSSION

Impacts have been invoked in many cases to explain thermal metamorphism and melting seen in meteorites (e.g., Schulz et al. 2009, 2010, 2012; Rubin 1995, 2003, 2004; Weirich et al. 2010; Wittmann et al. 2010). In particular, late-stage thermal events—those that occurred  $>5$  Myr after CAI formation—are probably the result of impacts, as SLRs are expected to have been extinct by then, and thus unable to be significant sources of heat at that time. Previous work had shown that subcatastrophic impacts cannot be responsible for global-scale heating of the type seen in meteoritic samples (Keil et al. 1997), but can produce the peak temperatures and cooling rates observed in meteorites on a local scale (Davison et al. 2012a). These previous studies, however, focused on impacts into “cold” planetesimals—those that retained no heat from SLRs.

The number of late-stage heating events recorded by meteorites that must be explained by impacts provides evidence that such events were frequent during the early evolution of the solar system. Indeed, such evidence of early collisions is consistent with models of planet formation. That is, collisional evolution models for the asteroid belt predict that the current size-frequency distribution of the asteroid belt was established no later than approximately 500 Myr after the solar system formed (O'Brien and Sykes 2011) and that a given body experienced approximately 50% of the impacts it will see in its lifetime in the first approximately 100 Myr with the greatest impact rate corresponding to the first approximately 10–20 Myr (Davison et al. 2013).

During this time of high impact rates, planetesimals thermally evolved (heated, were kept warm, and then cooled) from the decay of SLRs, most notably  $^{26}\text{Al}$ . This heat dramatically affected the outcome of an impact event and the postimpact structure of the remaining planetesimal, with hotter materials able to flow more readily under the stresses that they experienced during the various stages of crater formation (Ohnaka 1995; Collins et al. 2004). We have shown here that high preimpact temperatures in a target planetesimal resulted in hot material from the deep interior being brought to, and flowing out over, the surface of the planetesimal. This exposure of warmed materials, which would have otherwise remained buried in an unimpacted planetesimal, led to much more rapid cooling of the displaced materials. Cooling rates increased measurably in much larger fractions of the planetesimal than were heated by the impact, implying that the major effect of impacts would be to accelerate the loss of heat from a target body, rather than to deposit heat.

All of the impacts considered here were subcatastrophic, with the largest impact considered (10 km impactor at  $4 \text{ km s}^{-1}$ ) having an energy that was approximately 1% the disruption energy threshold for the target. Despite being subcatastrophic, this single impact had important effects on the thermal evolution of a significant fraction of the target, particularly if the impact happened in the first 20 Myr of solar system history. Given that an approximately 100 km radius planetesimal, roughly the size of the H chondrite parent body predicted by the onion-shell models, would experience approximately 300–1000 collisions during the first 100 Myr with a cumulative energy of 10–100 times the largest impact considered here (Davison et al. 2013), the cumulative effects of such events on the long-term thermal evolution of the parent body could be significant. One of the key factors in setting the full long-term effects is the timing of the impacts, which would vary across bodies (Davison et al. 2013). If

impacts were important in shaping the thermal evolution of H chondrites, for example, accelerating the cooling of type 4/5 meteorites as suggested by Scott et al. (2011), then this would probably indicate that the H chondrite parent body experienced an impact of the type considered here in the first approximately 20 Myr of its evolution. If impacts were not responsible for shaping any of the properties of these meteorites, it either means that the meteorites are coming from a region far from an impact site (such as the antipode) or it means that any major impacts that the H chondrite body experienced occurred late in its evolution. Future work, including determining the thermochronometry of more H chondrites, should allow us to better understand the physical evolution of this singular body.

While we have considered a variety of impact scenarios in this work, further efforts are needed to fully understand every role that impacts played in shaping the early geochemical and geophysical evolution of solar system bodies and the scales of these effects. Smaller impacts are likely to be much more frequent than those considered here, although their effects would be limited to correspondingly smaller volumes of the target and confined to the surface regions. Any heated material in these impacts would cool very rapidly compared with those materials considered here. Future efforts should be dedicated to understanding how these smaller impacts may have cumulatively processed potential meteoritic samples. Oblique impacts should be considered in the future, as those occurring at very shallow angles have been shown to affect a much smaller fraction of mass than head-on impacts (Davison et al. 2012b). Furthermore, here we limited our consideration to subcatastrophic impacts, but catastrophic impacts would deposit much more heat (Davison et al. 2010) while also producing a myriad of much smaller remnants that would evolve very quickly compared with the undisturbed target. As such impacts may have played a role in producing meteorites, such as the iron IABs and winonaites (e.g., Benedix et al. 2000), similar impact scenarios may help explain particular features in the meteorite record.

Despite the need for further studies, the conclusions reached here appear robust. The bombardment of early planetesimals led to significant thermal metamorphism in target materials immediately around the site of impact. Much more importantly, however, the cratering process in planetesimals warmed by the decay of SLRs would lead to the exposure of otherwise deeply buried materials, mobilizing this warm material, and bringing it to the surface. As a result, impacts in the early stages of planetary accretion, particularly in the first 20–30 Myr, probably played a greater role in cooling young planetesimals than heating.

*Acknowledgments*—We are grateful to the referees, Alan Rubin, Ed Scott, and Jay Melosh, and associate editor Adrian Brearley for insightful comments and suggestions that improved this manuscript. FJC and TMD were supported by grants NNX09AG13G and NNX12AQ06G from NASA PG&G. DPO acknowledges support from grant NNX09AE36G from NASA PG&G. GSC and TMD also acknowledge funds from STFC grant number ST/J001260/1.

*Editorial Handling*—Dr. Adrian Brearley

## REFERENCES

- Amsden A. A., Ruppel H. M., and Hirt C. W. 1980. SALE: A simplified ALE computer program for fluid flow at all speeds. Los Alamos National Laboratories Report LA-8095:101p.
- Barnes J. and Hut P. 1986. A hierarchical  $O(N \log N)$  force-calculation algorithm. *Nature* 324:446–449.
- Benedix G. K., McCoy T. J., Keil K., and Love S. G. 2000. A petrologic study of the IAB iron meteorites: Constraints on the formation of the IAB-winonaite parent body. *Meteoritics & Planetary Science* 35:1127–1141.
- Bennett M. E. III and McSween H. Y. Jr. 1996. Revised model calculations for the thermal histories of ordinary chondrite parent bodies. *Meteoritics & Planetary Science* 31:783–792.
- Benz W., Cameron A. G. W., and Melosh H. J. 1989. The origin of the Moon and the single-impact hypothesis III. *Icarus* 81:113–131.
- Bland P. A., Howard L. E., Prior D. J., Wheeler J., Hough R. M., and Dyl K. A. 2011. Earliest rock fabric formed in the solar system preserved in a chondrule rim. *Nature Geoscience* 4:244–247.
- Blum J. and Wurm G. 2008. The growth mechanisms of macroscopic bodies in protoplanetary disks. *Annual Review of Astronomy and Astrophysics* 46:21–56.
- Carslaw H. S. and Jäger J. C. 1959. *Conduction of heat in solids* (2nd ed.). Oxford: Clarendon Press.
- Castillo-Rogez J. C. and McCord T. B. 2010. Ceres' evolution and present state constrained by shape data. *Icarus* 205:443–459.
- Collins G. S., Melosh H. J., and Ivanov B. A. 2004. Modeling damage and deformation in impact simulations. *Meteoritics & Planetary Science* 39:217–231.
- Collins G. S., Melosh H. J., and Wünnemann K. 2011a. Improvements to the  $\epsilon$ - $\alpha$  porous compaction model for simulating impacts into high-porosity solar system objects. *International Journal of Impact Engineering* 38:434–439.
- Collins G. S., Davison T. M., and Ciesla F. J. 2011b. Numerical simulations of sub-catastrophic porous planetesimal collisions (abstract #1933). 42nd Lunar and Planetary Science Conference. CD-ROM.
- Crawford D. A. 2010. Parallel n-body gravitational interaction in CTH for planetary defense and large impact simulations (abstract #155). Proceedings of the 11th Hypervelocity Impact, Symposium.
- Cuzzi J. N., Hogan R. C., and Shariff K. 2008. Toward planetesimals: Dense chondrule clumps in the protoplanetary nebula. *The Astrophysical Journal* 687:1432–1447.
- Davison T. M., Collins G. S., and Ciesla F. J. 2010. Numerical modelling of heating in porous planetesimal collisions. *Icarus* 208:468–481.
- Davison T. M., Ciesla F. J., and Collins G. S. 2012a. Post-impact thermal evolution of porous planetesimals. *Geochimica et Cosmochimica Acta* 95:252–269.
- Davison T. M., Ciesla F. J., and Collins G. S. 2012b. The effect of impact obliquity on porous planetesimal collisions (abstract #1235). 43rd Lunar and Planetary Science Conference. CD-ROM.
- Davison T. M., O'Brien D. P., Ciesla F. J., and Collins G. S. 2013. The early impact histories of meteorite parent bodies. *Meteoritics & Planetary Science* 48:1894–1918. doi:10.1111/maps.12193.
- Elkins-Tanton L. T., Weiss B. P., and Zuber M. T. 2011. Chondrites as samples of differentiated planetesimals. *Earth and Planetary Science Letters* 305:1–10.
- Ghosh A. and McSween H. Y. 1998. A thermal model for the differentiation of asteroid 4 Vesta, based on radiogenic heating. *Icarus* 134:187–206.
- Ghosh A. and McSween H. Y. Jr. 1999. Temperature dependence of specific heat capacity and its effect on asteroid thermal models. *Meteoritics & Planetary Science* 34:121–127.
- Ghosh A., Weidenschilling S. J., McSween H. Y. Jr., Rubin A., and McSween H. Y. 2006. Asteroidal heating and thermal stratification of the asteroidal belt. In *Meteorites and the early solar system II*, edited by Lauretta D. S. Tucson, Arizona: University of Arizona Press. pp. 555–566.
- Grimm R. E. and McSween H. Y. 1993. Heliocentric zoning of the asteroid belt by aluminum-26 heating. *Science* 259:653–655.
- Harrison K. P. and Grimm R. E. 2010. Thermal constraints on the early history of the H-chondrite parent body reconsidered. *Geochimica et Cosmochimica Acta* 74:5410–5423.
- Henke S., Gail H. P., Trieloff M., Schwarz W. H., and Kleine T. 2012. Thermal evolution and sintering of chondritic planetesimals. *Astronomy & Astrophysics* 537:A45.
- Hevey P. J. and Sanders I. S. 2006. A model for planetesimal meltdown by  $^{26}\text{Al}$  and its implications for meteorite parent bodies. *Meteoritics & Planetary Science* 41:95–106.
- Ivanov B. A., Deniem D., and Neukum G. 1997. Implementation of dynamic strength models into 2D hydrocodes: Applications for atmospheric breakup and impact cratering. *International Journal of Impact Engineering* 20:411–430.
- Jacobsen B., Yin Q.-Z., Moynier F., Amelin Y., Krot A. N., Nagashima K., Hutcheon I. D., and Palme H. 2008.  $^{26}\text{Al}$ - $^{26}\text{Mg}$  and  $^{207}\text{Pb}$ - $^{206}\text{Pb}$  systematics of Allende CAIs: Canonical solar initial  $^{26}\text{Al}/^{27}\text{Al}$  ratio reinstated. *Earth and Planetary Science Letters* 272:353–364.
- Keil K., Stoeffler D., Love S. G., and Scott E. R. D. 1997. Constraints on the role of impact heating and melting in asteroids. *Meteoritics & Planetary Science* 32:349–363.
- Kleine T., Touboul M., van Orman J. A., Bourdon B., Maden C., Mezger K., and Halliday A. N. 2008. Hf W thermochronometry: Closure temperature and constraints on the accretion and cooling history of the H chondrite parent body. *Earth and Planetary Science Letters* 270:106–118.
- Leinhardt Z. M. and Stewart S. T. 2009. Full numerical simulations of catastrophic small body collisions. *Icarus* 199:542–559.

- Love S. G. and Ahrens T. J. 1996. Catastrophic impacts on gravity dominated asteroids. *Icarus* 124:141–155.
- Melosh H. J. 1979. Acoustic fluidization: A new geologic process? *Journal of Geophysical Research* 84:7513–7520.
- Melosh H. J. 1983. Acoustic fluidization. *American Scientist* 71:158–165.
- Melosh H. J. and Ivanov B. A. 1999. Impact crater collapse. *Annual Review of Earth and Planetary Sciences* 27:385–415.
- Melosh H. J., Ryan E. V., and Asphaug E. 1992. Dynamic fragmentation in impacts: Hydrocode simulation of laboratory impacts. *Journal of Geophysical Research* 97:14,735–14,759.
- O'Brien D. P. and Sykes M. V. 2011. The origin and evolution of the asteroid belt—Implications for Vesta and Ceres. *Space Science Reviews* 163:41–61.
- Ohnaka M. 1995. A shear failure strength law of rock in the brittle–plastic transition regime. *Geophysical Research Letters* 22:25–28.
- Opeil C. P., Consolmagno G. J., and Britt D. T. 2010. The thermal conductivity of meteorites: New measurements and analysis. *Icarus* 208:449–454.
- Pierazzo E., Artemieva N., Asphaug E., Baldwin E. C., Cazamias J., Coker R., Collins G. S., Crawford D. A., Davison T. M., Elbeshausen D., Holsapple K. A., Housen K. R., Korycansky D. G., and Wünnemann K. 2008. Validation of numerical codes for impact and explosion cratering: Impacts on strengthless and metal targets. *Meteoritics & Planetary Science* 43:1917–1938.
- Qin L., Dauphas N., Wadhwa M., Masarik J., and Janney P. E. 2008. Rapid accretion and differentiation of iron meteorite parent bodies inferred from  $^{182}\text{Hf}$   $^{182}\text{W}$  chronometry and thermal modeling. *Earth and Planetary Science Letters* 273:94–104.
- Rubin A. E. 1995. Petrologic evidence for collisional heating of chondritic asteroids. *Icarus* 113:156–167.
- Rubin A. E. 2003. Chromite-plagioclase assemblages as a new shock indicator; Implications for the shock and thermal histories of ordinary chondrites. *Geochimica et Cosmochimica Acta* 67:2695–2709.
- Rubin A. E. 2004. Postshock annealing and postannealing shock in equilibrated ordinary chondrites: Implications for the thermal and shock histories of chondritic asteroids 1. *Geochimica et Cosmochimica Acta* 68:673–689.
- Rubin A. E. and Jones R. H. 2003. Spade: An H chondrite impact-melt breccia that experienced post-shock annealing. *Meteoritics & Planetary Science* 38:1507–1520.
- Sahijpal S. and Gupta G. 2011. Did the carbonaceous chondrites evolve in the crustal regions of partially differentiated asteroids? *Journal of Geophysical Research* 116:E06004.
- Sahijpal S., Soni P., and Gupta G. 2007. Numerical simulations of the differentiation of accreting planetesimals with  $^{26}\text{Al}$  and  $^{60}\text{Fe}$  as the heat sources. *Meteoritics & Planetary Science* 42:1529–1548.
- Schulz T., Münker C., Palme H., and Mezger K. 2009. Hf-W chronometry of the IAB iron meteorite parent body. *Earth and Planetary Science Letters* 280:185–193.
- Schulz T., Münker C., Mezger K., and Palme H. 2010. Hf-W chronometry of primitive achondrites. *Geochimica et Cosmochimica Acta* 74:1706–1718.
- Schulz T., Upadhyay D., Münker C., and Mezger K. 2012. Formation and exposure history of non-magmatic iron meteorites and winonaites: Clues from Sm and W isotopes. *Geochimica et Cosmochimica Acta* 85:200–212.
- Scott E. R. D., Krot T. V., Goldstein J. I., and Taylor G. J. 2011. Thermal and impact history of H chondrites: Was the onion shell structure punctured by impacts during metamorphism? *Meteoritics & Planetary Science Supplement* 74:5516.
- Shoemaker E. M. 1962. Interpretation of lunar craters. In *Physics and astronomy of the Moon*, edited by Kopal Z. New York: Academic Press. pp. 283–359.
- Taylor G. J., Maggiore P., Scott E. R. D., Rubin A. E., and Keil K. 1987. Original structures, and fragmentation and reassembly histories of asteroids—Evidence from meteorites. *Icarus* 69:1–13.
- Trieloff M., Jessberger E. K., Herrwerth I., Hopp J., Fiéni C., Ghélis M., Bourot-Denise M., and Pellas P. 2003. Structure and thermal history of the H-chondrite parent asteroid revealed by thermochronometry. *Nature* 422:502–506.
- Walsh K. J., Morbidelli A., Raymond S. N., O'Brien D. P., and Mandell A. M. 2011. A low mass Mars from Jupiter's early gas-driven migration. *Nature* 475:206–209.
- Weirich J. R., Wittmann A., Isachsen C. E., Rumble D., Swindle T. D., and Kring D. A. 2010. The Ar-Ar age and petrology of Miller Range 05029: Evidence for a large impact in the very early solar system. *Meteoritics & Planetary Science* 45:1868–1888.
- Wittmann A., Swindle T. D., Cheek L. C., Frank E. A., and Kring D. A. 2010. Impact cratering on the H chondrite parent asteroid. *Journal of Geophysical Research (Planets)* 115:07009.
- Wünnemann K., Collins G. S., and Melosh H. J. 2006. A strain-based porosity model for use in hydrocode simulations of impacts and implications for transient crater growth in porous targets. *Icarus* 180:514–527.
- Wünnemann K., Collins G. S., and Osinski G. R. 2008. Numerical modelling of impact melt production in porous rocks. *Earth and Planetary Science Letters* 269:530–539.
- Yomogida K. and Matsui T. 1984. Multiple parent bodies of ordinary chondrites. *Earth and Planetary Science Letters* 68:34–42.
-